Electronic Supplementary Material (ESI) for Chemical Communications.

Rapid access to RNA resonances by proton-detected solid-state NMR at >100 kHz MAS

Alexander Marchanka, Jan Stanek, Guido Pintacuda, Teresa Carlomagno

Electronic Supplementary information

Contents

1. *Sample preparation*

Deuterated L7Ae protein was expressed in *Escherichia coli* (deuterated M9 medium) and purified over a Ni-Nta column followed by an anion exchange column, as reported elsewhere.[1-3]

Uniformly ^{1}H,^{13}C,^{15}N labeled 26mer Box C/D RNA and 26mer Box C/D RNA with ^{2}H,^{12}C,^{14}N-C,U,A and ^{1}H,^{13}C,^{15}N-G were prepared by *in vitro* transcription with T7 polymerase produced in house. All NTPs were purchased from Silantes.

The L7Ae–Box C/D RNA complex was assembled from protein and RNA in a 1:1 ratio and purified by size exclusion chromatography. Afterwards, the protein-RNA complex was concentrated to 20 mg/ml in buffer with 25 mM HEPES and 120 mM sodium chloride at pH 7.5 in 100% H_2O or 90% D_2O and subsequently mixed with equal amount of precipitation solution (100 mM sodium acetate, 30% PEG 400 in 100 mM HEPES, pH 7.5 in 100% H_2O or 90% D_2O), as reported previously.[3,4]

The sample was micro-crystallized by slow precipitation using a SpeedVac concentrator at room temperature for approximately 2 hours. The complex precipitated at half volume as expected.

The precipitate was packed by ultracentrifugation at 120000 × g for 1 h at 4 °C directly into the 0.7 mm NMR rotor using a sample packing tool from Giotto Biotech.[5,6] In total, 0.5 mg of protein-RNA complex were packed into the 0.7 mm rotor, which corresponds to about 200 μg of uniformly ^{13}C,^{15}N labeled RNA.

2. *NMR spectroscopy*

Samples and equipment. All presented spectra were acquired for samples originally dissolved in a 9:1 D_2O:H_2O solution, except those shown in Fig. S2 and S1c,d,e,f. The experiments were performed on a spectrometer at $\omega_{0H}/2\pi$ = 1 GHz (static field of B_0 = 23.5 T) equipped with a commercial Bruker 0.7-mm HCN probe, with the exception of ^{13}C-^{1}H CP-HSQC spectra shown in Fig. 1b, and ^{1}H and ^{13}C T_2' and $T_{1\rho}$ measurements summarized in Fig. 1c and Fig. S2, which were recorded at $\omega_{0H}/2\pi$ = 800 MHz (a static field of B_0 = 18.8 T) equipped with a commercial Bruker 0.7-mm HCND probe. 4D HCCH-TOCSY was recorded at both B_0 fields, but with different acquisition parameters as detailed in Table S1.

Magic-angle spinning. Rotors were spun at the magic-angle at the following frequency: 111 kHz for CP-HSQC spectra shown in Fig. S1c,d and both ribose- and base-tuned (H)NCH spectra shown in Fig. 3; 108 and 107 kHz for the HCCH-TOCSY spectra acquired on the 1 GHz and 800 MHz spectrometers, respectively; 100 kHz for the (H)NCCH-TOCSY (in Fig. S3) and CP-HSQC spectra shown in Fig. S1a,b,e,f; 109, 60, 40 and 20 kHz for the CP-HSQC spectra shown in Fig. 1b; from 40 to 109 every 10 kHz for the $T_1\rho$ measurements summarized in Fig. S2. Magic-angle was carefully adjusted before every measurement by maximizing the signal in the ^{13}C-^{1}H CP-HSQC experiment followed by a constant-time ^{1}H echo period.

Temperature control. The sample temperature was maintained at approximately 280 K using a Bruker cooling unit (BCUII) with a sufficient flow of dry N_2 gas. The sensor indicated the temperature after the bearing, drive and cooling gases are mixed. The following values were requested, depending on a MAS frequency and an amount of associated frictional heating: 255, 260, 265, 270, 275 and 280 for MAS rate of 111 to 107, 100, 90, 80, 70, and 60 to 20 kHz, respectively.

Shimming. The field homogeneity was controlled with a sample of adamantane using a one-pulse ^{13}C spectrum with low-power swept-TPPM ^{1}H decoupling. Full-width at half-height below 5 Hz was always observed after shim adjustment for the downfield ^{13}C line.

Field stability. The experiments were acquired without the field lock except those performed on the 800 MHz spectrometer with a HCND 4-channel 0.7-mm probe (on a sample precipitated from a 9:1 D_2O:H_2O solution). Field stability was monitored using 1D ^{1}H spectra before and after the experiments, and, whenever necessary, the uniformly sampled 3D spectra were corrected for magnet drift using in-house written nmrPipe[7] scripts. 4D NUS data were only corrected in the directly detected dimension.

Spin decoupling. WALTZ-16[8] decoupling with $\gamma B_1/2\pi$ = 10 kHz was used for ^{1}H-decoupling during indirect heteronuclear evolution periods. WALTZ-16 was also used for ^{15}N decoupling during evolution of ^{13}C spins, and the B_1 strength was 10 kHz except for (H)CH and (H)NCH experiment for bases, where $\gamma B_1/2\pi$ = 20 kHz was necessary to cover the chemical shift range of N1, N3, N7 and N9 spins coupled to C2, C6 and C8 spins. DIPSI-3[9] decoupling with $\gamma B_1/2\pi$ = 20 kHz was used for ^{13}C decoupling during either ^{1}H or ^{15}N evolution periods, including acquisition of ^{1}H signal. In the particular case of spectra acquired at MAS frequency of 20 kHz, SPINAL-64[10] with RF amplitude of 100 kHz and pulse length of 4.8μs was applied for ^{1}H decoupling during ^{13}C transverse magnetization periods.

Solvent suppression. The MISSISSIPPI[11] scheme was employed to suppress H_2O or HDO residual signal during z-storage of ^{13}C magnetization. 50 ms (or 200 ms for the sample in 100% H_2O) of RF irradiation with $\gamma B_1/2\pi$ of approximately 45-50 kHz was used.

TOCSY mixing. WALTZ-16[8] scheme was employed to isotropically mix ^{13}C z-magnetization in the ribose spin system. The duration of mixing was set to 25 ms to maximize the signal transferred from ^{13}C5' to ^{13}C1' as monitored on a series of 2D (H)C(C)H-TOCSY experiments. RF strength was set to $\gamma B_1/2\pi$ = 25 kHz. A *z*-filter (a delay) of 5 ms before and after WALTZ-16 mixing was applied.

Inter-scan delay. A delay of 0.9-1.0 s was applied for optimal recovery of ^{1}H *z*-magnetization.
High-power RF pulses. The typical durations (and RF field strengths) of "hard" pulses were 2.5 μs (100 kHz), 5.5 μs (45.5 kHz) and 3.0 μs (83.3 kHz) for ^{1}H, ^{15}N and ^{13}C nuclei, respectively.

Cross-polarization (CP) conditions. The shapes, offsets, durations and powers employed for cross-polarization transfers are summarized in Table S2.

Parameters and issues specific to experiments are discussed in the following:

^{13}C-^{1}H CP-HSQC (Fig. 2). The experiment follows, with little modifications, the scheme proposed by Rienstra and co-workers[12,13]. In particular, protonated base ^{13}C spins (C2, C6 and C8) were recorded separately from ribose ^{13}C spins (C1'-C5') to avoid off-resonance effects and line shape distortions. For this reason, selective ^{13}C refocusing pulses from BURP family[14] were applied to eliminate signals outside of the region of interest. A pulse of 350/250 μs and max. B_1 amplitude of 17.9/25.0 kHz was used for the selection of base/ribose resonances, respectively. The ^{1}H, ^{15}N and ^{13}C carrier frequency was set to 4.8, 160 and either 80 (for ribose ^{13}C) or 145 ppm (for base ^{13}C), respectively. Quadrature-detection in ω_1 (^{13}C) was accomplished using the States-TPPI procedure[15] by simultaneous incrementation of t_1 and the phase of ^{13}C RF irradiation during the $^{1}H \rightarrow {}^{13}C$ CP (in steps of $\pi/2$). The following phase cycle was used: $\varphi_1 = y, -y$; $\varphi_2 = 2(x), 2(y), 2(-x), 2(-y)$; $\varphi_3 = 8(x), 8(-x)$; $\varphi_{REC} = 2(y, -y, -y, y), 2(-y, y, y, -y)$; where φ_1 is the phase of the first ^{1}H $\pi/2$ pulse, φ_2 is the phase of the selective ^{13}C pulse (ReBURP), φ_3 is the phase of ^{1}H RF during the $^{1}H \rightarrow {}^{13}C$ CP, and φ_{REC} denotes the receiver phase.

^{1}H bulk T_2' measurement. The results shown in Fig. 1c were obtained with a slightly modified ribose- or base-selective ^{13}C-^{1}H CP-HSQC experiment, where a time-incremented ^{1}H echo is performed directly before the acquisition of ^{1}H signal. The signal was indirectly sampled to at least $2T_2'(^{1}H)$ to ensure fidelity of the exponential fit (minor deviations are observed as the experiment yields intensity-averaged bulk T_2').

^{13}C bulk T_2' measurement (Fig. S2). The experiment also derives from base-selective ^{13}C-^{1}H CP-HSQC, in which ^{13}C chemical evolution in t_1 is replaced by a time-incremented ^{13}C echo with a selective ^{13}C refocusing pulse. The measurements were performed for $^{13}C6/8$ only, since, in contrast to ribose carbon spins, C8 nuclei do not show significant homonuclear *J*-couplings, and C6 can be easily decoupled from C5 spins with a selective ReBURP pulse (of 769 μs duration and max. RF field of 8.15 kHz).

^{1}H bulk $T_{1\rho}$ measurement (Fig. S3). The experiment is derived from ^{13}C-^{1}H CP-HSQC by the insertion of a ^{1}H spin-lock rectangular pulse of adjustable duration and RF field strength directly after the first ^{1}H pulse. (Note that for more precise site-specific studies, this spin-lock pulse should rather be placed directly before acquisition.)

^{13}C bulk $T_{1\rho}$ measurement (Fig. S3). Similarly, a ^{13}C-^{1}H CP-HSQC pulse scheme is used, with an additional ^{13}C spin-lock rectangular pulse of adjustable duration and RF field strength. This pulse is performed just after the $^{1}H \rightarrow {}^{13}C$ CP.

(H)NCH-ribose tuned (Fig. 3). First, ^{15}N spins are polarized from distant protons with a long-range CP, and their chemical shift is evolved (t_1). Subsequently, magnetization is transferred to $^{13}C1'$ with a selective CP to avoid the concurrent pathway $^{15}N1 \rightarrow {}^{13}C_{base}$.

After the evolution of ^{13}C1' (t_2), magnetization is flipped-back for a *z*-storage, followed by a solvent suppression period. Finally, the ^{13}C $\pi/2$ pulse re-excites ^{13}C spins, which are then transferred with a short CP to directly bonded ^{1}H for detection. Despite the relatively small chemical shift difference between C1' and C6/8 spins (40-60 ppm corresponding to 10-15 kHz on a 1 GHz spectrometer) compared to the ^{13}C RF field strength required to trigger ^{15}N→^{13}C CP at ultrafast MAS, the selectivity towards C1' can be obtained with either on-resonance CP (i.e. at the offset of C1', or below) and a decreasing ^{15}N RF strength, or with an off-resonance CP (i.e. at the offset of C6/8 or above) and a increasing ^{15}N RF strength during CP. In both cases, the effective nutation frequency for ^{13}C1' $\omega_{eff} = \sqrt{\omega_1^2 + (\Delta\Omega/(2\pi))^2}$ matches the DQ CP condition ($\omega_{eff}{}^{C} + \omega^{N} = \omega_R$) before ^{13}C6/8 spins. ^{1}H, ^{15}N and ^{13}C carrier signal was set to 4.8, 160 and 89 ppm, respectively. Quadrature-detection in ω_1 (^{15}N) and ω_2 (^{13}C) was accomplished using the States-TPPI protocol by simultaneous incrementation of t_1 and the phase of ^{15}N RF irradiation during the ^{1}H→^{15}N CP (in steps of $\pi/2$), and concurrent incrementation of t_2 and the decrementation (in steps of $-\pi/2$) of the phase of the ^{13}C $\pi/2$ pulse after t_2. The following phase cycle was used: φ_1 = *y*, *-y*; φ_2 = 2(*x*), 2(*-x*); φ_3 = 4(*y*), 4(*-y*); φ_{REC} = *y, -y, -y, y*, *-y, y, y, -y*; where φ_1 is the phase of ^{15}N RF during the ^{1}H→^{15}N CP, φ_2 is the phase of ^{13}C RF during ^{15}N→^{13}C CP, φ_3 is the phase of the first ^{1}H $\pi/2$ pulse, and φ_{REC} is the receiver phase.

(H)NCH-base tuned (Fig. 3). The pulse sequence is identical to the (H)NCH experiment for ribose spins, and the selectivity is obtained with the ^{13}C carrier shifted to approximately 144 ppm. Either CP on-resonance with ^{13}C6/8 and decreasing ^{15}N RF field strength, or an off-resonance CP (e.g. at the ^{13}C effective offset of ^{13}C1' or below) and an increasing ^{15}N RF strength can be used for the ^{15}N→^{13}C CP. Note that the leak of magnetization to C2/C4 carbons (for pyrimidine/purine residues) cannot be prevented. Additionally, the initial polarization is smaller for purine base ^{15}N9 spins, since H8 protons polarize both nearby N7 and N9 spins. One observes additional pathways from N1 and N3 to C2-H2 in Adenine bases. To avoid confusion between N7 and N9 one has to ensure sufficient spectral window in ω_1. In our setup, we decided for a reasonable window of 100 ppm ^{15}N which folds N1, N3 and N7 to an upfield edge of ω_1, so that they appear at lower frequencies than N1 and N9.

HCCH-TOCSY (Fig. 3). The pulse scheme has been derived from 3D (H)CCH- and H(C)CH-TOCSY experiments described previously for proteins.[16] To minimize the spectral windows in the indirect dimensions, the ^{1}H, ^{15}N and ^{13}C carrier signal was set to 5.6, 160 and 80 ppm, respectively, with only minor adverse effects on the solvent suppression. No additional means were applied to obtain selectivity for ribose ^{13}C spins, therefore a low intensity signal of base ^{1}H6/8 spins can be observed in the respective region of the directly observed dimension. The following phase cycle was used: φ_1 = *x*, *-x*; φ_2 = 2(*x*), 2(*-x*); φ_3 = 4(*x*), 4(*-x*); φ_{REC} = *x, -x, -x, x*, *-x, x, x, -x*; where φ_1 is the phase of ^{13}C RF during the ^{1}H→^{13}C CP, φ_2 is the phase of ^{1}H RF during ^{1}H→^{13}C CP, φ_3 is the phase of the ^{13}C $\pi/2$ pulse before t_3, and φ_{REC} is the receiver phase. Quadrature-detection in ω_1 (^{1}H), ω_2 (^{13}C) and ω_3 (^{13}C) was accomplished using the States-TPPI protocol by a simultaneous incrementation of either t_1, t_2 or t_3, and either decrementation of the phase φ_2, or incrementation of the phase φ_1, or the phase φ_3 (in steps of $-\pi/2$ or $+\pi/2$), respectively. 3000 $t_1/t_2/t_3$ NUS points (1.7%) were randomly chosen out of the full 3D grid, using exponentially weighted distribution functions (with assumed T_2* of 1.8 and 2.7 ms for ^{1}H and ^{13}C, respectively) and otherwise default settings of the build-in TopSpin utility, originally provided by Orekhov and co-workers.[17] The experiment was

performed also at the 800 MHz spectrometer, with truncated indirect evolution times to favor sensitivity over resolution. In this case, 4320 NUS points (26.3%) were randomly chosen using exponentially weighted distribution of points with the approximate T_2* of 2.7 and 3.0 ms for ^{1}H and ^{13}C dimensions, respectively.

(H)NCCH-TOCSY (Fig. S4). Magnetization is transferred from ^{1}H to ^{15}N through a long CP step. After evolution of N1/N9 frequencies in t_1, a specific CP brings the magnetization back to C1' spins, whose chemical shift is recorded in t_2. The WALTZ-16 mixing spreads the magnetization to all ribose carbons, whose frequency is encoded in t_3. Finally, a short CP transfer brings the magnetization back to ^{1}H for detection. A short evolution time on ^{15}N (t_{1max} = 3.0 ms) was sufficient to separate purine from pyrimidine resonances and at the same time optimize sensitivity. A selective ^{13}C refocussing pulse (ReBURP) is applied after t_2 to select only ^{13}C1' spins and suppress the residual signal of ^{13}C8/6 at this stage. The duration (369.7 μs) and maximum RF field strength (14.52 kHz) of this pulse are adjusted to yield approximately 50 ppm ^{13}C bandwidth. ^{1}H, ^{15}N and ^{13}C carrier signals were set to 4.8, 160 and 80 ppm, respectively. The selective ^{15}N→^{13}C CP is performed as described for the ribose-tuned (H)NCH experiment. The following phase cycle was used: φ_1 = *x*, *-x*; φ_2 = 2(*x*), 2(*y*); φ_3 = 4(*y*), 4(*-y*); φ_{REC} = *y, -y, -y, y, -y, y, y, -y*; where φ_1 is the phase of ^{15}N RF during the ^{1}H→^{15}N CP, φ_2 is the phase of the ^{13}C ReBURP pulse after t_2, φ_3 is the phase of the first ^{1}H π/2 pulse, and φ_{REC} is the receiver phase. Quadrature-detection in ω_1 (^{15}N), ω_2 (^{13}C1') and ω_3 (^{13}C1'-5') was accomplished using the States-TPPI protocol by a simultaneous incrementation of either t_1, t_2 or t_3, and either incrementation of the phase φ_1, or the phase of the "hard" ^{13}C π/2 pulse before the TOCSY mixing, or by decrementation of the phase of the "hard" ^{13}C π/2 pulse after t_3 (in steps of +π/2 or –π/2), respectively. 1400 $t_1/t_2/t_3$ NUS points (4.9%) were randomly chosen out of the full 3D grid, using exponentially weighted distribution functions (assuming T_2* of 3.2, 2.7 and 2.4 ms for ^{15}N, ^{13}C1' and ^{13}C1'-5', respectively).

Data processing and analysis. ^{13}C chemical shifts were referenced as described by Morcombe and Zilm,[18] ^{15}N and ^{1}H chemical shifts were referenced indirectly using chemical shift referencing ratios from.[19] The spectra were processed with NMRPipe[7] and visualized with CcpNmr Analysis.[20] NMRFAM-Sparky[21] was used to elucidate the resonance limiting line widths, defined as full widths at half-height of a sufficiently sampled signal, with no window function applied in the processing. NUS data were converted using nmrPipe and processed with the cleaner4d program from the SSA package.[22]

Table S1. Acquisition parameters of the recorded spectra

Spectrum ↓		Indirect evolution times, ms				Acq, ms	Spectral widths, kHz (ppm)					Scans per point	NUS points	Exp. Time h
Dimension→		^{13}C	^{13}C	^{1}H	^{15}N	^{1}H	^{13}C	^{13}C	^{1}H	^{15}N	^{1}H acq			
2D HSQC ribose-selective Fig. 2		8.4	–	–	–	10.0	15.1 (60)	–	–	–	100 (100)	48	–	3.8
2D HSQC (800) Fig. 1	MAS rate:													
	109 kHz	7.8	–	–	–	8.0	9.3	–	–	–	32.1	64	–	2.7
	60 kHz	7.8				8.0	9.3				32.1	64		2.7
	40 kHz	7.8				8.0	9.3				32.1	224		9.5
	20 kHz	6.0				8.0	20.1				64.1	256		50.0
2D HSQC base-selective Fig. 2		8.0	–	–	–	10.0	10.1 (40)	–	–	–	100 (100)	96	–	4.8
3D (H)NCH ribose-tuned Fig. 3		5.0	-	4.9	-	6.7	3.0 (12)	–	–	4.1 (40)	100 (100)	32	–	12
3D (H)NCH base-tuned Fig. 3		4.9	-	4.9	-	6.7	5.5 (22)	–	–	10.1 (100)	100 (100)	16	–	26.5
4D HCCH-TOCSY (1000) Fig. 3		8.0	8.0	-	3.6	8.0	12.6 (50)	12.6 (50)	5.0 (5.0)	–	100 (100)	8	3000	68
4D HCCH-TOCSY (800) Fig. 3		4.0	4.0	-	3.0	8.0	9.3 (46)	9.3 (46)	4.0 (4.0)	–	32.1 (40)	8	4320	90
4D (H)NCCH-TOCSY Fig. S4		5.0	5.0	3.0	-	2.0	7.5 (30)	12.6 (50)	–	4.1 (40)	100 (100)	32	1400	110

Table S2. Summary of cross-polarization conditions

	Transfer	Contact time, ms	Type	Max (average) RF strength, kHz		RF pulse shape	
2D HSQC ribose-selective	^{1}H→^{13}C	0.45	ZQ(n=1)	127.9	25.0	Linear ramp up ±5%	Rectangle
	^{13}C→^{1}H	0.17	ZQ(n=1)	116.7	25.0	Linear ramp up ±5%	Rectangle
2D HSQC base-selective	^{1}H→^{13}C	0.45	ZQ(n=1)	127.9	25.0	Linear ramp up ±5%	Rectangle
	^{13}C→^{1}H	0.17	ZQ(n=1)	116.7	25.0	Linear ramp up ±5%	Rectangle
3D (H)NCH ribose-tuned	^{1}H→^{15}N	12.0	ZQ(n=1)	139.9	30.3	Linear ramp up ±5%	Rectangle
	^{15}N→^{13}C	20.0	DQ(n=1)	40.4	70.0	Tangential down ±10% [a]	Rectangle Off-resonance -49 ppm (at 50 ppm ^{13}C)
	^{13}C→^{1}H	0.24	DQ(n=1)	75.0	53.0 (38.4)	Rectangle	Linear ramp down ±38%
3D (H)NCH base-tuned	^{1}H→^{15}N	13.0	ZQ(n=1)	139.9	30.3	Linear ramp up ±5%	Rectangle
	^{15}N→^{13}C	14.0	DQ(n=1)	42.0	70.0	Tangential down ±10% [a]	Rectangle On-resonance (at 144 ppm ^{13}C)
	^{13}C→^{1}H	0.24	DQ(n=1)	75.0	53.0 (38.4)	Rectangle	Linear ramp down ±38%
4D HCCH-TOCSY (1000)	^{1}H→^{13}C	0.20	DQ(n=1)	37.3 (24.2)	86.7	Linear ramp down ±54%	Rectangle
	^{13}C→^{1}H	0.17	DQ(n=1)	86.7	36.7 (23.9)	Rectangle	Linear ramp up ±54%
4D HCCH-TOCSY (800)	^{1}H→^{13}C	0.30	DQ(n=1)	44.9 (28.1)	84.1	Linear ramp down ±60%	Rectangle

	$^{13}C \rightarrow {}^{1}H$	0.19	DQ(n=1)	84.1	40.2 (25.1)	Rectangle	Linear ramp up ±60%
4D (H)NCCH-TOCSY	$^{1}H \rightarrow {}^{15}N$	13.0	ZQ(n=1)	122.7	28.1	Linear ramp up ±5%	Rectangle
	$^{15}N \rightarrow {}^{13}C$	12.0	DQ(n=1)	43.0	65.0	Tangential up ±10% [a]	Rectangle Off-resonance +60 ppm (at 130 ppm ^{13}C)
	$^{13}C \rightarrow {}^{1}H$	0.24	DQ(n=1)	75.5	44.8 (32.5)	Rectangle	Linear ramp down ±38%

[a] Tangential amplitude modulation $S(x)=1 \pm 0.1 \tan[\pi\alpha(x - 0.5)] / \tan(0.5\pi\alpha)$, where $\alpha = 7/9$ (effectively, the tangent is truncated at 70 deg at the edges) and x varies from 0 to 1 throughout the CP. The ramp with increasing amplitude (with + in the formula) leads to off-resonance $^{15}N \rightarrow {}^{13}C$ CP, while with the ramp "down" (with – in the formula) the on-resonance $^{15}N \rightarrow {}^{13}C$ CP occurs first.

Table S3. Fourier processing parameters of the recorded spectra

Spectrum ↓	Digital resolution					Window function [b]				
Dimension→	^{13}C	^{13}C	^{1}H	^{15}N	^{1}H acq	^{13}C	^{13}C	^{1}H	^{15}N	^{1}H acq
2D HSQC ribose-selective	1024	–	–	–	8192	QSINE3	–	–	–	QSINE3
2D HSQC ribose-selective (800) at different MAS rates (Fig. 1)	512	–	–	–	4096	QSINE3	–	–	–	QSINE3
2D HSQC base-selective	512	–	–	–	8192	QSINE3	–	–	–	QSINE3
3D (H)NCH ribose-tuned	128	–	–	128	4096	QSINE2	–	–	GM -60Hz/0.2	QSINE3
3D (H)NCH base-tuned	128	–	–	256	4096	QSINE2	–	–	GM -60Hz/0.2	QSINE3
4D HCCH-TOCSY (1000) [a]	256	256	64	–	2048	QSINE3	QSINE3	QSINE3	–	QSINE3
4D HCCH-TOCSY (800) [a]	256	256	64	–	2048	QSINE3	QSINE3	QSINE3	–	QSINE3
4D (H)NCCH-TOCSY [a]	256	384	–	192	2048	NO [c]	–	NO [c]	NO [c]	QSINE3

[a] For the NUS experiments, the parameters refer to the Fourier processing after the reconstruction of missing signal points

[b] The terms denote: QSINEq – squared shifted sine bell function: $w(t) = \sin [\pi (1 - 1 / q)(t / t_{max}) + \pi / q]^2$ (where q = 2 and 3 for QSINE2 and QSINE3, respectively). GM a/b – mixed Lorentian-Gaussian function $w(t) = \exp [(-\pi a) t + (\pi a / (2 b t_{max}) t^2)]$; here a = -60 Hz and b = 0.2.

[c] Apodization function is not mandatory for the data sampled with exponentially weighted distribution of points

3. *Aggregated ^{1}H, ^{13}C and ^{15}N chemical shifts*

Table S4. Isotropic chemical shifts of the 26mer Box C/D RNA in the L7Ae-Box C/D RNA complex, as obtained in this study. Nucleotide spin systems are assigned in this study. The sequence specific assignment, shown here for clarity, is taken from ref 1c.[a,b]

	Isotropic chemical shifts, ppm												
	H1'	H2'	H3'	H4'	H5'/H5''	H6/H8	C1'	C2'	C3'	C4'	C5'	C6/C8	N1/N9
C2	-	-	-	-	-	*7.9*	-	-	-	-	-	*140.7*	*151.8*
U3	5.6	*4.2*	*4.3*	*4.4*	*4.4/4.*	7.4	94.9	*75.6*	*71.7*	*83.1*	63.9	140.2	145.2
G4	5.7	5.0	4.9	4.9	4.4/4.0	8.1	90.1	75.9	79.5	88.2	67.8	139.2	166.9
A5	5.7	4.5	4.9	4.9	4.4/4.2	7.7	88.2	78.4	79.8	83.5	70.3	139.9	167.2
G6	6.8	4.9	4.7	5.0	4.8/4.5	8.4	92.7	76.0	77.2	83.5	70.9	139.1	170.9
C7	6.0	4.5	4.6	4.5	4.7/4.2	8.4	93.8	75.3	72.1	81.9	64.3	142.6	152.4
U8	5.6	-	*4.7*	-	-	8.3	93.7	-	*71.8*	-	-	142.9	147.9
C9	5.7	-	-	-	-	7.4	93.7	-	-	-	-	140.2	152.0
G10	5.7	-	-	-	-	7.5	93.9	-	-	-	-	136.3	171.1
A*/G*[c]	5.4	*4.2*	*4.5*	*4.3*	*4.3*	-	93.3	*75.6*	*72.2*	*81.9*	*64.1*	-	170.6
G14	-	-	-	-	-	*8.0*	-	-	-	-	-	*137.5*	-
A15	6.0	4.5	4.7	4.6	4.6/3.9	*7.9*	92.7	75.6	72.2	81.6	64.2	*139.5*	171.7
G16	5.8	4.5	-	4.5	4.6/4.1	*7.7*	92.5	75.4	*72.1*	81.6	64.3	-	*171.3*
C17	5.6	4.6	4.5	*4.5*	*4.5*	7.4	93.5	75.6	71.7	*81.5*	*64.4*	139.4	150.9
A18	6.3	4.1	4.8	4.8	4.6/4.4	8.1	94.1	76.6	72.6	81.6	64.5	138.8	173.1
A19	4.7	4.8	4.6	3.4	4.4/3.9	7.9	89.8	72.2	78.5	85.1	67.3	146.0	164.9
U20	6.2	4.8	4.5	5.3	4.1/4.0	8.5	89.5	75.3	80.5	84.2	69.5	147.2	147.7
G21	6.1	5.3	5.0	5.2	4.5	8.4	87.5	77.5	80.0	87.4	68.2	139.2	168.6
A22	5.8	5.0	4.6	*4.8*	4.6/4.2	7.9	92.4	75.9	72.3	82.9	65.8	140.2	170.3
U23	4.9	4.4	4.5	4.4	4.7/4.1	7.6	93.0	74.6	72.2	82.4	63.0	140.5	144.9
G24	-	-	-	-	-	-	-	-	-	-	-	-	-

[a] Assignments derived from only one spectrum are shown in italics.

[b] Resonances assigned previously in ^{13}C-detected experiments but not assigned in this work are not shown.[2]

[c] „A*/G*“ denotes unresolved resonances belonging to nucleotides 11-13 in the loop and/or G14/G24

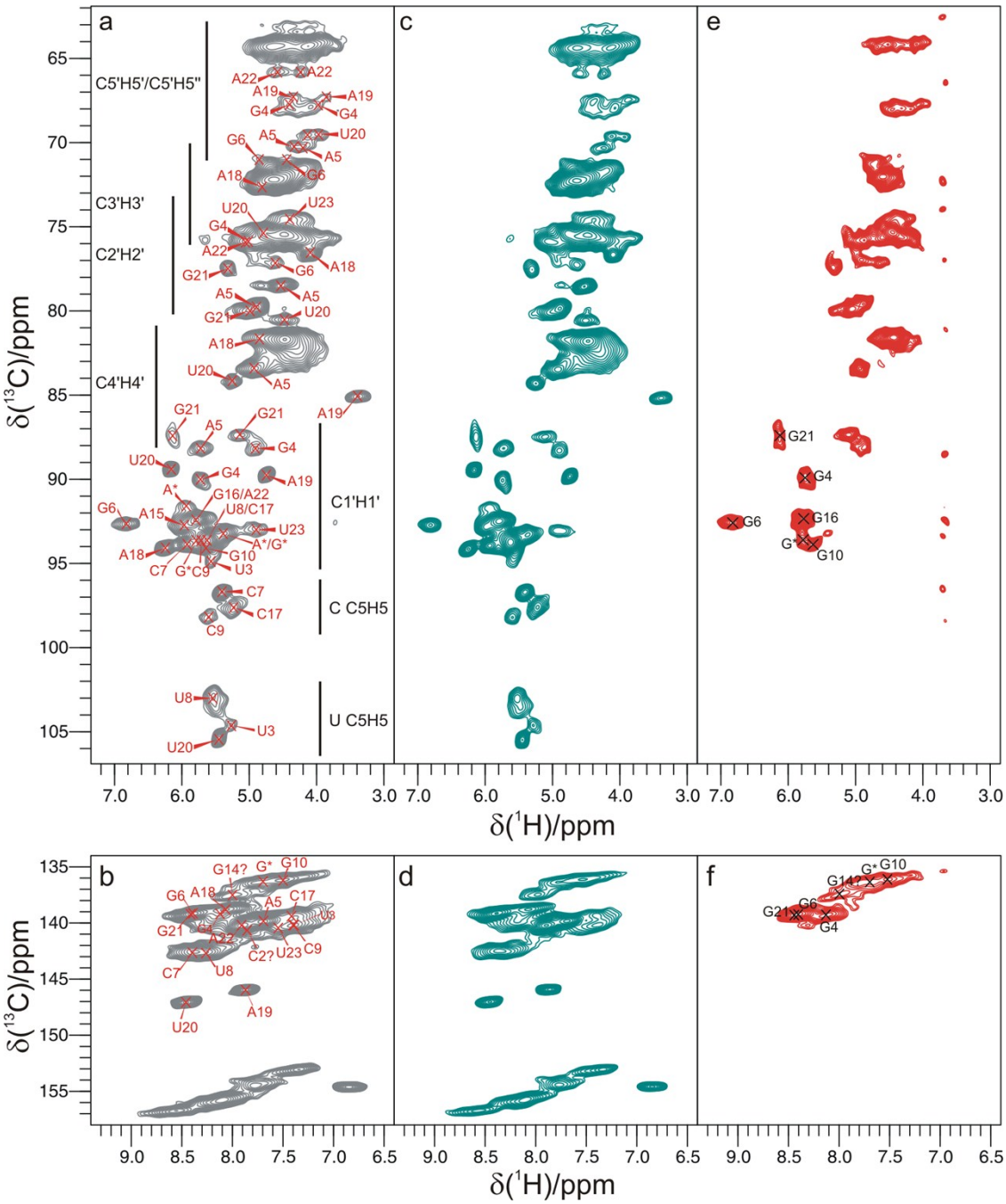

Fig. S1. 2D CP-HSQC ribose (a, c) and base (b, d) spectra of the L7Ae – Box C/D 26mer RNA complex consisting of uniformly ^{1}H,^{13}C,^{15}N labeled 26mer Box C/D RNA and ^{2}H,^{12}C,^{14}N L7Ae in 100% H_2O (a, b) or 90% D_2O (c, d). 2D CP-HSQC ribose (e) and base (f) spectrum of the L7Ae – Box C/D 26mer RNA complex consisting of ^{2}H,^{12}C,^{14}N-C,U,A and ^{1}H,^{13}C,^{15}N-G labeled 26mer Box C/D RNA and ^{2}H,^{12}C,^{14}N L7Ae in 90 % D_2O.

4. *Base carbon refocused transverse relaxation*

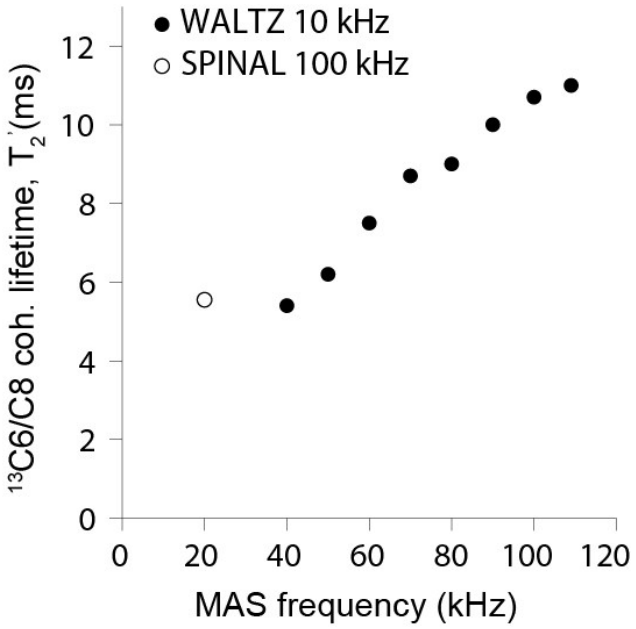

Fig. S2. The bulk refocused transverse relaxation time of ^{13}C6 and ^{13}C8 spins, measured at different MAS frequencies (i.e. at 20 and from 50 to 110 every 10 kHz) on a 800 MHz spectrometer. The effects of homonuclear couplings (for ^{13}C6) were eliminated by a selective refocusing pulse, as described in section 2 of this Supplement. Low-power WALTZ-16 ^{1}H decoupling with $h\gamma B_1/2\pi$ = 10 kHz was applied at all MAS frequencies except for 20 kHz. Exponential decay was assumed in all cases.

5. *Proton and carbon rotating-frame relaxation*

Rotating-frame relaxation times are particularly important in solids since they determine (among other factors) the efficiency of cross-polarization. In the present study, we frequently use CP transfers of extended durations, e.g. for a long-range ^{1}H→^{15}N (up to 13 ms) and one-bond ^{15}N→^{13}C transfer (up to 20 ms). Also, ^{13}C $T_1\rho$ translates into efficiency of TOCSY mixing (here 25 ms was used), employed in HCCH and (H)NCCH experiments. For this reason, we investigated here the dependence of ^{1}H and ^{13}C $T_1\rho$ of ribose spins on the MAS frequency (between 40 and 110 kHz).

Rotating-frame relaxation is dependent on the B_1 field strength, and prominently enhanced close to the rotary-resonance conditions ($\gamma B_1/2\pi$ = ½ ω_R, ω_R, $2\omega_R$, etc.). To simplify this complex phenomenon, we measured first the signal intensity of the ribose resonances when applying a constant-time spin-lock pulse (of 15 ms and 10 ms for ^{13}C and ^{1}H spin-lock, respectively) at varied RF field strength in the range permitted by the RF properties of the 0.7 mm MAS probe. The resulting spectra were integrated over the entire region of H1' resonances, and integrals normalized to the intensity of a reference (H)CH 1D signal at the given MAS frequency.

Fig. S3a demonstrates that ^{13}C $T_1\rho$ relaxation is attenuated as the MAS rate increases, with improved separation between dips corresponding to the consecutive resonance-rotary conditions. ^{1}H rotating-frame relaxation shows a similar dependence (Fig. S3c); however, for B_1 field strengths above 130-150 kHz similar rates are obtained regardless of MAS rate (unless a resonance-rotary condition is approached). In practice, such strong B_1 fields cannot easily be used when spinning rotors at moderate MAS rates in probes with RF coils of larger diameters, due to the large current amplitude required. Therefore, ssNMR spectroscopy at MAS frequency > 100 kHz has the additional

advantage to easily reach this optimal regime of ^{1}H B_1 and thus extend the spin-locked relaxation time.

Additionally, we recorded time-series at selected RF field strengths to allow a crude estimation of relaxation times at the given conditions (Fig. S3b,d). We focused our attention on the case of $\gamma B_1/2\pi$ = ¼ ω_R as it is always far from the rotary-resonance condition, and additionally at one constant B_1 field strength: 40 kHz for ^{13}C and 150 kHz for ^{1}H. We abstained from fitting these time-series due to frequent deviations from the exponential decay.

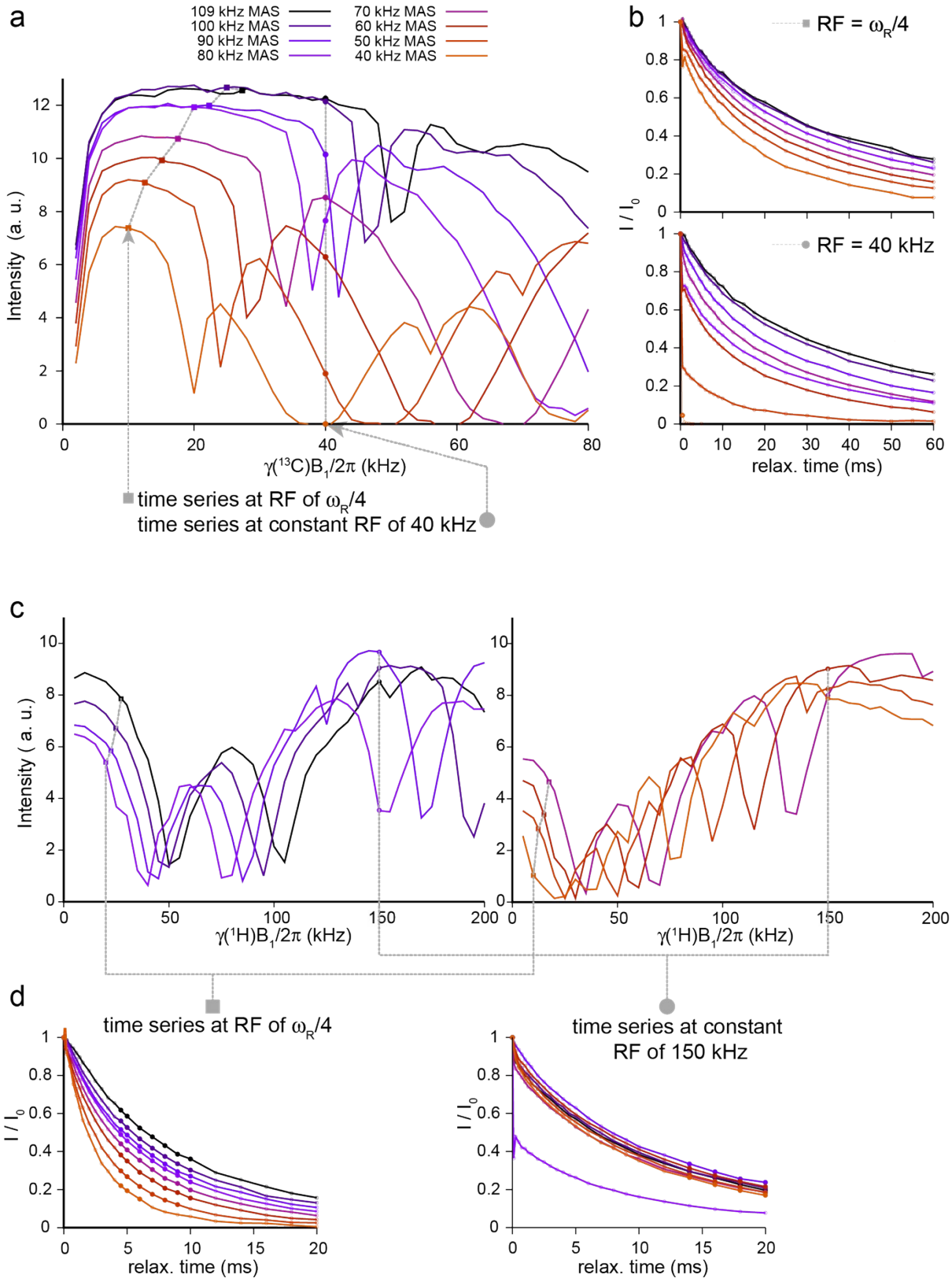

Fig. S3. (a) Integrated and normalized intensity of ^{1}H ribose signals in the ^{13}C-^{1}H CP-HSQC experiment with a 15 ms ^{13}C spin-lock pulse of B_1 field strength varied from 2 to 80 kHz (every 2 kHz). The data was recorded on a 800 MHz spectrometer and at MAS frequency ranging from 40 to 109 kHz (every 10 kHz). (b) Normalized time-series (decays) recorded at the ^{13}C RF field strength of one fourth of MAS frequency and at the constant RF amplitude of 40 kHz. (c) Integrated and normalized intensity of ^{1}H ribose signals in ^{13}C-^{1}H CP-HSQC experiment with a 10 ms ^{1}H spin-lock pulse of B_1 field strength varied from 5 to 200 kHz (every 5 kHz). The curves for MAS frequencies are separated to improve readability. (d) Normalized

integrals of signal intensities for a time-series (decays) with the ^{1}H RF field strength of either one fourth of MAS frequency, or at the constant B_1 field strength of 150 kHz.

6. *4D (H)NCCH experiment*

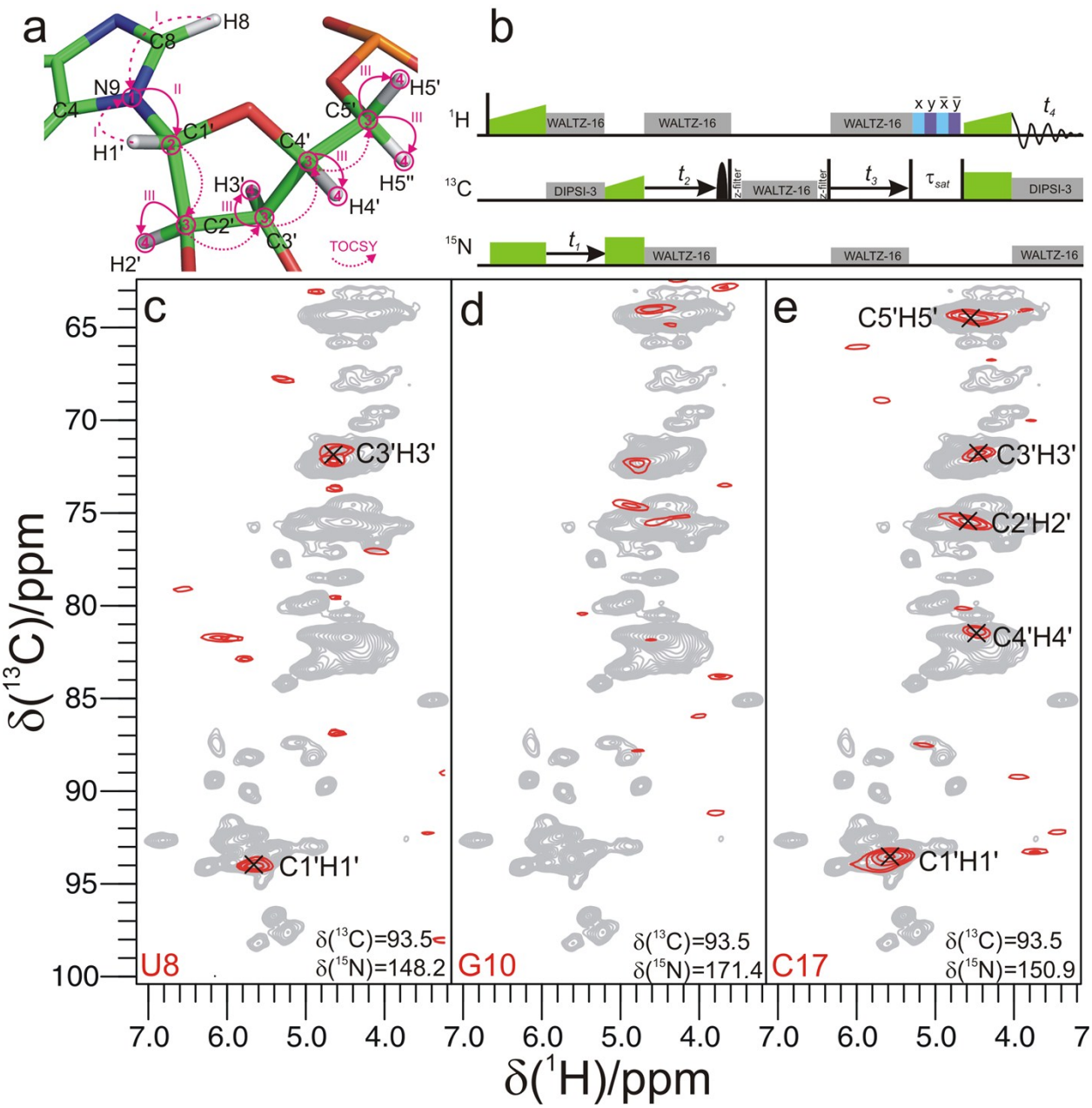

Fig. S4. Magnetization transfer (a) and radiofrequency irradiation scheme b) for the (H)NCCH-TOCSY experiment. Arabic numbers in a) correspond to spectral dimensions (t_1-t_4) in the pulse scheme (b), and roman numbers indicate the CP transfers. Representative 2D planes from the 4D experiment showing the spin systems of (c) U8, (d) G10, and (e) C17.^{13}C and ^{15}N frequencies are indicated in each panel. For reference, in panels (c-f) the *red* contours of the 4D (H)NCCH-TOCSY spectrum are overlaid onto the 2D CP-HSQC spectrum (in *grey*). The spectrum was recorded on a 1 GHz spectrometer and at 100 kHz MAS.

7. References

1. S. Jehle, M. Falb, J. P. Kirkpatrick, H. Oschkinat, B. J. van Rossum, G. Althoff and T. Carlomagno, *J. Am. Chem. Soc.*, 2010, **132**, 3842-3846.
2. S. Asami, M. Rakwalska-Bange, T. Carlomagno and B. Reif, *Angew. Chem. Int. Ed.*, 2013, **52**, 2345-2349.
3. A. Marchanka, B. Simon, G. Althoff-Ospelt and T. Carlomagno, *Nat. Commun.*, 2015, **6**, Article number: 7024
4. A. Marchanka, B. Simon and T. Carlomagno, *Angew. Chem. Int. Ed.*, 2013, **52**, 9996-10001.
5. I. Bertini, C. Luchinat, G. Parigi, E. Ravera, B. Reif and P. Turano, *Proc. Natl. Acad. Sci. USA*, 2011, **108**, 10396-10399.
6. A. Boeckmann, C. Gardiennet, A. Hunkeler, A. Loquet, G. Pintacuda, L. Emsley, B. H. Meier and A. Lesage, *J. Biomol. NMR*, 2009, **45**, 319.
7. F. Delaglio, S. Grzesiek, G. W. Vuister, G. Zhu, J. Pfeifer and A. Bax, *J. Biomol. NMR*, 1995, **6**, 277-293.
8. A. J. Shaka, J. Keeler, T. Frenkiel and R. Freeman, *J. Magn. Reson.*, 1983, **52**, 335-338.
9. A. J. Shaka, C. J. Lee and A. Pines, *J. Magn. Reson.*, 1988, **77**, 274-293.
10. B. M. Fung, A. K. Khitrin and K. Ermolaev, *J. Magn. Reson.*, 2000, **142**, 97-101.
11. D. H. Zhou and C. M. Rienstra, *J. Magn. Reson.*, 2008, **192**, 167-172.
12. D. H. Zhou, G. Shah, M. Cormos, C. Mullen, D. Sandoz and C. M. Rienstra, *J. Am. Chem. Soc.*, 2007, **129**, 11791-11801.
13. D. H. Zhou, J. J. Shea, A. J. Nieuwkoop, W. T. Franks, B. J. Wylie, C. Mullen, D. Sandoz and C. M. Rienstra, *Angew. Chem. Int. Ed.*, 2007, **46**, 8380-8383.
14. H. Geen and R. Freeman, *J. Magn. Reson.*, 1991, **93**, 93-141.
15. D. J. States, R. A. Haberkorn and D. J. Ruben, *J. Magn. Reson.*, 1982, **48**, 286-292.
16. J. Stanek, L. B. Andreas, K. Jaudzems, D. Cala, D. Lalli, A. Bertarello, T. Schubeis, I. Akopjana, S. Kotelovica, K. Tars, A. Pica, S. Leone, D. Picone, Z. Q. Xu, N. E. Dixon, D. Martinez, M. Berbon, N. El Mammeri, A. Noubhani, S. Saupe, B. Habenstein, A. Loquet and G. Pintacuda, *Angew. Chem. Int. Ed.*, 2016, **55**, 15503-15509.
17. V. Y. Orekhov, I. Ibraghimov and M. Billeter, *J. Biomol. NMR*, 2003, **27**, 165-173.
18. C. R. Morcombe and K. W. Zilm, *J. Magn. Reson.*, 2003, **162**, 479-486.
19. J. L. Markley, A. Bax, Y. Arata, C. W. Hilbers, R. Kaptein, B. D. Sykes, P. E. Wright and K. Wüthrich, *Eur. J. Biochem*, 1998, **256**, 1-15.
20. W. F. Vranken, W. Boucher, T. J. Stevens, R. H. Fogh, A. Pajon, M. Llinas, E. L. Ulrich, J. L. Markley, J. Ionides and E. D. Laue, *Proteins: Struct., Funct., Bioinf.*, 2005, **59**, 687-696.
21. W. Lee, M. Tonelli and J. L. Markley, *Bioinformatics*, 2015, **31**, 1325-1327.
22.J. Stanek, R. Augustyniak and W. Kozminski, *J. Magn. Reson.*, 2012, **214**, 91-102.